



OBMeshfree: An Optimization-Based Meshfree Solver for Nonlocal Diffusion and Peridynamics Models

Yiming Fan¹ · Huaiqian You¹ · Yue Yu¹

Received: 26 November 2022 / Accepted: 15 March 2023 / Published online: 14 April 2023
© The Author(s), under exclusive licence to Springer Nature Switzerland AG 2023

Abstract

We present OBMeshfree, an Optimization-Based Meshfree solver for compactly supported nonlocal integro-differential equations (IDEs) that can describe material heterogeneity and brittle fractures. OBMeshfree is developed based on a quadrature rule calculated via an equality constrained least square problem to reproduce exact integrals for polynomials. As such, a meshfree discretization method is obtained, whose solution possesses the asymptotically compatible convergence to the corresponding local solution. Moreover, when fracture occurs, this meshfree formulation automatically provides a sharp representation of the fracture surface by breaking bonds, avoiding the loss of mass. As numerical examples, we consider the problem of modeling both homogeneous and heterogeneous materials with nonlocal diffusion and peridynamics models. Convergence to the analytical nonlocal solution and to the local theory is demonstrated. Finally, we verify the applicability of the approach to realistic problems by reproducing high-velocity impact results from the Kalthoff-Winkler experiments. Discussions on possible immediate extensions of the code to other nonlocal diffusion and peridynamics problems are provided. OBMeshfree is freely available on GitHub (Fan et al. [1]).

Keywords Bond-based peridynamics · Meshfree method · Asymptotic compatibility · Convergence rates · Heterogeneous Material

1 Introduction

Nonlocal models such as nonlocal diffusion and peridynamics provide a description of governing laws in terms of integral operators rather than classical differential operators [2–8]. They can describe phenomena not well represented by classical partial differential equations (PDEs), especially on problems characterized by long-range interactions

✉ Yue Yu
yuy214@lehigh.edu
Yiming Fan
yif319@lehigh.edu
Huaiqian You
huy316@lehigh.edu

¹ Department of Mathematics, Lehigh University, Bethlehem, PA, USA

and discontinuities [2, 9, 10]. As a result, applications of nonlocal models span a large spectrum of scientific and engineering problems, including subsurface transport [11–15], phase transitions [16–18], image processing [19–22], multiscale and homogenized systems [23–29], turbulence [30, 31], stochastic processes [32–34], and fracture mechanics [7, 35, 36].

In this work, we consider nonlocal models that are characterized by a general heterogeneous nonlocal operator of the form:

$$\mathcal{L}_\delta[u](\mathbf{x}, t) := \int_{B_\delta(\mathbf{x})} K(\mathbf{x}, \mathbf{y})(u(\mathbf{y}, t) - u(\mathbf{x}, t))d\mathbf{y}, \quad \text{with } K(\mathbf{x}, \mathbf{y}) := \varpi(\mathbf{x}, \mathbf{y})C(\mathbf{x}, \mathbf{y})\gamma(\mathbf{x}, \mathbf{y}).$$

where u is the solution we seek, $\gamma(\mathbf{x}, \mathbf{y}) := \gamma_\delta(|\mathbf{x} - \mathbf{y}|)$ is a (possibly singular) radial kernel which for fixed \mathbf{x} is supported on the ball of radius δ , $B_\delta(\mathbf{x})$, and the two-point functions $\varpi(\mathbf{x}, \mathbf{y})$ and $C(\mathbf{x}, \mathbf{y})$ allow for the description of material heterogeneity while preserving the physical consistency. δ defines the extent of nonlocal interactions, which is also referred to as a horizon. This integral form allows for the description of long-range interactions and reduces the regularity requirements on problem solutions, and hence enhances the accuracy of their modeling representations by generalizing the space of admissible solutions, which can feature discontinuities. Another important feature of such models is that when the classical continuum models still apply and with proper definitions of $\varpi(\mathbf{x}, \mathbf{y})$ and $C(\mathbf{x}, \mathbf{y})$, these nonlocal models can revert back to classical continuum models with heterogeneous material properties, as $\delta \rightarrow 0$.

When discretizing the nonlocal models, it is desired to preserve the corresponding local limit under refinement grid size $h \rightarrow 0$, since analyzing consistency in the limit to the local solution provides a mathematically unambiguous means to understand accuracy and physical compatibility. Such a property is termed asymptotically compatible (AC) [37].¹ In recent years, there has been significant work toward establishing such discretizations [37–47]. Broadly, strategies either involve adopting traditional finite element shape functions and carefully performing geometric calculations to integrate over relevant horizon/element subdomains, or adopt a strong-form meshfree discretization where particles are associated with abstract measure. The former is more amenable to mathematical analysis due to a better variational setting, while the latter is simple to implement and generally faster [48, 49].

In this paper we focus on the meshfree approach and approximate the heterogeneous nonlocal operator as:

$$\mathcal{L}_\delta[u](\mathbf{x}_i, t) \approx \mathcal{L}_{\delta, h}[u](\mathbf{x}_i, t) := \sum_{j \neq i} K(\mathbf{x}_i, \mathbf{x}_j)(u(\mathbf{x}_j, t) - u(\mathbf{x}_i, t))\omega_{ij},$$

where the quadrature weights ω_{ij} are associated with a local neighborhood of particles for each discretization point \mathbf{x}_i , generated by local optimizations to make the approximation rule exact for certain classes of functions. By defining the averaged material property field $K(\mathbf{x}, \mathbf{y})$ as an analog of a series of two springs connecting the two points, our recent work [45, 50–54] has provided theoretical analysis and numerical verifications on the AC property on this optimization-based quadrature rule for heterogeneous materials [51, 52].

¹ For nonlocal models one often refines both δ and h at the same rate under so-called δ -convergence [72], to allow scalable implementations. Although in the literature a scheme is termed AC if it recovers the solution whenever $\delta, h \rightarrow 0$, in this work we adopt a practical setting and only require the δ -convergence for AC.

In this paper, we will provide an open-source meshfree solver and demonstrations of its convergence properties on various examples. To achieve a convergent simulation, the AC property to the local limit is only one important ingredient. Besides the consistency to the local limit, two additional features are desired in our nonlocal problem solver. Firstly, in peridynamics problems, one of its main appeals is to handle fracture problems, where free surfaces are associated with the evolution of a fracture surface. To achieve numerical consistency for problems involving fracture, one must also consider the interplay between consistency of quadrature for discrete operators and the imposition of traction loads as fracture surfaces open up and evolve [55]. Second, in applications such as the particle systems with long-range interactions, the horizon size δ should be seen as a physical value and there is possibly no corresponding local limit. To preserve the physical consistency in such a scenario, the numerical convergence to the correct nonlocal limit when $h \rightarrow 0$ would be desired in the nonlocal problem solver.

Our goal is to demonstrate a comprehensive treatment of nonlocal quadrature rule, material heterogeneity, and evolving free surfaces, which is able to achieve numerical consistency to both local and nonlocal limits and capture material fracture. In particular, when no fracture occurs and the analytical solution is sufficiently smooth, the formulation should preserve the AC limit under δ -convergence and the consistency to the nonlocal limit as $h \rightarrow 0$. Moreover, when fracture occurs, the formulation should be able to capture the material damage and the evolving fracture surfaces via bond breaking. This practically means that one is able to incorporate all of the necessary ingredients to perform non-trivial simulations of fracture mechanics while maintaining a scalable implementation and guaranteeing convergence. To achieve these properties, our development has two steps. First, to handle material heterogeneity and free surfaces in such a way that one preserves a limit to the relevant local problem, a unified mathematical formulation is introduced. Then, to preserving the AC limit under δ -convergence and the consistency to the nonlocal limit as $h \rightarrow 0$, an optimization-based quadrature rule is employed. As a result, our method provides an efficient discretization with rigorous underpinnings for a class of nonlocal models featuring material heterogeneity and evolving fractures.

We remark that the paper is organized to first establish the mathematical formulations and provide a brief summary of theoretical underpinnings of the approach, while the second half focuses on a user manual for the code [1] together with demonstrations on several exemplar applications. Practitioner with more applied interests may skip the first part without issue. The paper is organized as follows.

We firstly recall the heterogeneous nonlocal diffusion and bond-based peridynamics problems in Sect. 2, and provide a unified mathematical formulation for handling material heterogeneity and fracture. In Sect. 3, the optimization-based quadrature rule is elaborated as a unified numerical approach for heterogeneous nonlocal diffusion and bond-based peridynamics, together with the treatment of material fracture. We also provide a summary of the rigorous convergence analysis for the optimization-based quadrature rule, verifying its consistency to the local limit when $h, \delta \rightarrow 0$, and to the nonlocal limit when $h \rightarrow 0$. Then, in Sect. 4 the main structure of OBMeshfree code is shown and each code component is discussed in detail. In Sect. 5, we demonstrate four examples as verifications and validations of the code, including three problems with manufactured solutions and one example on reproducing high-velocity impact results from the Kalthoff-Winkler experiment as an engineering-oriented problem. Section 6 summarizes our results and discusses future research.

2 Nonlocal Theory

In this section, we introduce the notation and describe the nonlocal models that will be useful throughout the following sections.

Let $\Omega \in \mathbb{R}^d$, $d = 1, 2, 3$, be a bounded open domain. We are interested in solving for functions $u : \Omega \rightarrow \mathbb{R}$ and $\mathbf{u} : \Omega \rightarrow \mathbb{R}^d$, solutions of nonlocal diffusion and nonlocal mechanics problems, respectively. Herein, $u(\mathbf{x})$ represents the concentration of a diffusive quantity in the nonlocal diffusion problem, and $\mathbf{u}(\mathbf{x})$ represents the displacement field of an object in mechanics. In nonlocal settings, every point in a domain interacts with a neighborhood of points. In this work, we further assume that such neighborhood is an Euclidean ball surrounding points in the domain, i.e., $B_\delta(\mathbf{x}) := \{\mathbf{y} \in \mathbb{R}^d : |\mathbf{y} - \mathbf{x}| \leq \delta\}$, where δ is the horizon. This assumption has implications on the concept of boundary conditions. In particular, unless otherwise stated, the boundary conditions should no longer be prescribed on the sharp interface, $\partial\Omega$, but on a collar of thickness of at least δ surrounding the domain Ω , that we refer to as the nonlocal volumetric boundary domain (or simply nonlocal boundary),

$$\mathcal{B}\Omega := \{\mathbf{x} \notin \Omega \mid \text{dist}(\mathbf{x}, \partial\Omega) < \delta\}.$$

This set consists of all points outside the domain that interact with points inside the domain. To define the nonlocal problems with general mixed boundary conditions, we further decompose the sharp interface $\partial\Omega$ into two parts: $\partial\Omega = \partial\Omega_D \cup \partial\Omega_N$, where $(\partial\Omega_D)^o \cap (\partial\Omega_N)^o = \emptyset$. To apply the nonlocal Dirichlet-type boundary condition, we assume that $\mathbf{u}(\mathbf{x}) = \mathbf{u}_D(\mathbf{x})$ are provided in a layer with non-zero volume outside Ω , while the free surface boundary condition is applied on the sharp interface $\partial\Omega_N$. To define a Dirichlet-type constraint, we denote

$$\mathcal{B}\Omega_D := \{\mathbf{x} \notin \Omega \mid \text{dist}(\mathbf{x}, \partial\Omega_D) < \delta\},$$

and assume that the value of \mathbf{u} is given on $\mathcal{B}\Omega_D$. For notation simplicity, we denote $\Omega_D := \Omega \cup \mathcal{B}\Omega_D$.

In this paper and the code [1], we focus on 2D problems ($d = 2$) and provide demonstrations with both static and dynamic examples, although the method is also applicable to 3D problems.

2.1 Nonlocal Diffusion Models

Nonlocal diffusion models have been employed in many applications [30, 56], and they are capable to describe the underlying phenomena when the classical Fick’s first law or standard Brownian motion fails [57–60]. Specifically, given a loading field f , the time-dependent nonlocal diffusion equation can be given as:

$$\frac{\partial u}{\partial t}(\mathbf{x}, t) - \mathcal{L}_{D\delta}[u](\mathbf{x}, t) = f(\mathbf{x}, t), \tag{1}$$

where the diffusion operator on scalar function $u : \mathbb{R}^d \rightarrow \mathbb{R}$ is defined as

$$\mathcal{L}_{D\delta}[u](\mathbf{x}, t) := 2 \int_{B_\delta(\mathbf{x})} A(\mathbf{x}, \mathbf{y}) \gamma(\mathbf{x}, \mathbf{y}) (u(\mathbf{y}, t) - u(\mathbf{x}, t)) d\mathbf{y} = f(\mathbf{x}, t), \quad \mathbf{x} \in \Omega. \tag{2}$$

Here, $A(\mathbf{x}, \mathbf{y}) \in [r, R]$, $r, R > 0$, is a uniformly bounded and continuous two-point function, describing the heterogeneous diffusion property. γ denotes a properly scaled kernel function which is assumed to satisfy:

$$\gamma(\mathbf{x}, \mathbf{y}) = \gamma_\delta(|\mathbf{x} - \mathbf{y}|) = \frac{1}{\delta^{d+2}} \gamma_1\left(\frac{|\mathbf{x} - \mathbf{y}|}{\delta}\right) = \frac{D_0}{\delta^{d+2-s} |\mathbf{x} - \mathbf{y}|^s}, \quad (3)$$

where γ_1 is a nonnegative and nonincreasing function, s is the order of the kernel singularity in γ , and there exists a positive constant $\zeta < 1$ satisfying $B_\zeta(\mathbf{0}) \subset \text{supp}(\gamma_1) \subset B_1(\mathbf{0})$ and $\int_{B_1(\mathbf{0})} \gamma_1(|\mathbf{z}|) |\mathbf{z}|^2 d\mathbf{z} = d$. Then, (1) can be seen as a nonlocal analog to the local diffusion equation.² In particular, when taking the local diffusion parameter field $a(\mathbf{x}) := A(\mathbf{x}, \mathbf{x})$ and consistent Dirichlet-type boundary conditions, it was shown in [51] that (1) is well-posed and converges to the classical diffusion equation

$$\frac{\partial u}{\partial t}(\mathbf{x}, t) - \mathcal{L}_D[u](\mathbf{x}, t) = f(\mathbf{x}, t), \quad \mathcal{L}_D[u](\mathbf{x}, t) := \nabla \cdot (a(\mathbf{x}) \nabla u(\mathbf{x}, t)), \quad (4)$$

as $\delta \rightarrow 0$. Therefore, in examples where only the local diffusion coefficient field $a(\mathbf{x})$ is provided, one can take the nonlocal diffusion coefficient as the harmonic mean of the local diffusion coefficient:

$$A(\mathbf{x}, \mathbf{y}) = 2 \left(\frac{1}{a(\mathbf{x})} + \frac{1}{a(\mathbf{y})} \right)^{-1}. \quad (5)$$

For further details, we refer interested readers to [51].

Here, we consider nonlocal diffusion problems with Dirichlet-type boundary conditions without loss of generality.³ That means, $\mathcal{B}\Omega = \mathcal{B}\Omega_D$ and a volume constraint $u_D : \mathcal{B}\Omega \times [0, T] \rightarrow \mathbb{R}$ is provided. Then, the nonlocal counterpart of a Dirichlet boundary condition for PDEs is applied as a volume constraint: $u(\mathbf{x}, t) = u_D(\mathbf{x}, t)$ for $(\mathbf{x}, t) \in \mathcal{B}\Omega \times [0, T]$. Although in Sect. 5 we only provide numerical verification for the convergence of numerical solutions in static cases, sample codes for both static and time-dependent nonlocal diffusion problems are provided in [1].

2.2 Peridynamics Models

The peridynamic theory provides a nonlocal mechanics model, which has been applied for material failure and damage simulation [2, 7, 61–64] and provided robust modeling capabilities for analysis of complex crack propagation phenomena, such as crack branching [35, 54, 65, 66], bridging, deflection and trapping [52, 67].

Consider a body occupying the domain Ω , the general peridynamic equation of motion for a point $\mathbf{x} \in \Omega$ and time $t \in [0, T]$ is

² Herein, we apply the assumptions in (3) so as to guarantee the compatibility of the nonlocal model and its local limit, in the limit of vanishing nonlocality, i.e., $\delta \rightarrow 0$. However, we point out that the optimization-based quadrature rule as well as the OBMeshfree package can be readily applied to more general kernels, such as the data-driven kernel developed in [29].

³ Neumann and Robin-type boundary conditions can be implemented with the quadrature rule provided by OBMeshfree, following [46, 47, 81]

$$\rho \frac{\partial^2 \mathbf{u}}{\partial t^2}(\mathbf{x}, t) - \mathcal{L}_{P_\delta}[\mathbf{u}](\mathbf{x}, t) = \mathbf{f}(\mathbf{x}, t),$$

where \mathcal{L}_{P_δ} is a nonlocal operator representing the peridynamic internal force density, ρ is the mass density, and \mathbf{f} is a prescribed body force density. As for the nonlocal diffusion problems, the nonlocal interactions in \mathcal{L}_{P_δ} are also restricted to the nonlocal neighborhood, $B_\delta(\mathbf{x})$, characterized by the horizon size δ . In this work, we focus on the bond-based peridynamic solid model [2, 45, 68], and take the peridynamics operator as:

$$\mathcal{L}_{P_\delta}[\mathbf{u}](\mathbf{x}, t) := c \int_{B_\delta(\mathbf{x})} \kappa(\mathbf{x}, \mathbf{y}) \gamma(|\mathbf{y} - \mathbf{x}|) \frac{(\mathbf{y} - \mathbf{x}) \otimes (\mathbf{y} - \mathbf{x})}{|\mathbf{y} - \mathbf{x}|^2} (\mathbf{u}(\mathbf{y}, t) - \mathbf{u}(\mathbf{x}, t)) d\mathbf{y}. \tag{6}$$

Here, γ is the kernel function as defined in (3), and the two-point functions $\kappa(\mathbf{x}, \mathbf{y})$ denote the (averaged) bulk modulus property.⁴ To recover parameters for linear elasticity when the nonlocal effects vanish, one should take $c = 24/5$ for $d = 2$, and $c = 6$ for $d = 3$ (see, e.g., [4, 45] for further details). Similar as in the nonlocal diffusion problems, in examples where only the local bulk modulus coefficient field $\kappa(\mathbf{x})$ is provided, we take the nonlocal bulk modulus coefficient as the harmonic mean of the local coefficient [67, 69, 70]:

$$\kappa(\mathbf{x}, \mathbf{y}) = 2 \left(\frac{1}{\kappa(\mathbf{x})} + \frac{1}{\kappa(\mathbf{y})} \right)^{-1}. \tag{7}$$

One of the main features of peridynamics is to handle fracture problems, where damage is incorporated into the peridynamic constitutive model by allowing the bonds of solid interactions to break irreversibly. Here we employ the critical stretch criterion where breakage occurs when a bond is extended beyond some predetermined critical bond deformed length [54, 71]. Then, this criterion is implemented by multiplying the pairwise force function with a history-dependent scalar Boolean function. In particular, to model brittle fracture, we break the bond between two material points, \mathbf{x} and \mathbf{y} , when the associated strain exceeds a critical strain threshold. A two-point Boolean state function $\theta(\mathbf{x}, \mathbf{y}, t)$ is defined and updated to describe the bond breakage through the crack growing

$$\theta(\mathbf{x}, \mathbf{y}, t) = \begin{cases} 1, & \text{if } S(\mathbf{x}, \mathbf{y}, \tau) \leq S_0(\mathbf{x}, \mathbf{y}), \forall \tau \leq t, \text{ and } \mathbf{y} \in B_\delta(\mathbf{x}) \cap \Omega_D, \\ 0, & \text{otherwise,} \end{cases} \tag{8}$$

where the associated strain S and the critical bond stretch S_0 related to material parameters are defined as [71]:

$$S(\mathbf{x}, \mathbf{y}, t) := \frac{\|u(\mathbf{y}, t) - u(\mathbf{x}, t) + \mathbf{y} - \mathbf{x}\| - \|\mathbf{y} - \mathbf{x}\|}{\|\mathbf{y} - \mathbf{x}\|},$$

$$S_0(\mathbf{x}, \mathbf{y}) := \begin{cases} \sqrt{\frac{\pi G(\mathbf{x}, \mathbf{y})}{3\kappa(\mathbf{x}, \mathbf{y})\delta}}, & 2D, \\ \sqrt{\frac{5G(\mathbf{x}, \mathbf{y})}{9\kappa(\mathbf{x}, \mathbf{y})\delta}}, & 3D, \end{cases} \tag{9}$$

where κ is the nonlocal bulk modulus coefficient.

⁴ In 2D problems, the bond-based peridynamics model is restricted with Poisson ratio $\nu = 1/4$ in the plane strain setting and $\nu = 1/3$ in the plane stress setting. In 3D problems one has a fixed Poisson ratio $\nu = 1/3$. Hence, the bulk modulus, κ , and the Young's modulus, E , can be converted from each other following $\kappa = \frac{E}{3(1-2\nu)}$.

In (9) $G(\mathbf{x}, \mathbf{y})$ is the averaged fracture energy defined via the arithmetic mean:

$$G(\mathbf{x}, \mathbf{y}) = \frac{1}{2}(G(\mathbf{x}) + G(\mathbf{y})). \quad (10)$$

Here, the averaged material properties definition in (7) and the averaged fracture energy definition in (10) are inspired by seeing the interaction between \mathbf{x} and \mathbf{y} as an analog of a series of two springs connecting the two points. Following a similar argument as in [52], one can show that when no fracture occurs and the local modulus field satisfies $\kappa \in C(\Omega \cup \bar{\mathcal{B}}\Omega)$, it is guaranteed that the nonlocal solution of (6) converges to the solution of a linear elastic model as $\delta \rightarrow 0$, hence it preserves the correct local limit.

In summary, with proper initial conditions and Dirichlet-type boundary condition in $\mathcal{B}\Omega_D$, we obtain a unified mathematical formulation for dynamic bond-based peridynamics for $\mathbf{x} \in \Omega$:

$$\rho \frac{\partial^2 \mathbf{u}}{\partial t^2}(\mathbf{x}, t) - c \int_{\mathcal{B}_\delta(\mathbf{x})} \theta(\mathbf{x}, \mathbf{y}, t) \kappa(\mathbf{x}, \mathbf{y}) \gamma(|\mathbf{y} - \mathbf{x}|) \frac{(\mathbf{y} - \mathbf{x}) \otimes (\mathbf{y} - \mathbf{x})}{|\mathbf{y} - \mathbf{x}|^2} (\mathbf{u}(\mathbf{y}, t) - \mathbf{u}(\mathbf{x}, t)) d\mathbf{y} = \mathbf{f}(\mathbf{x}, t). \quad (11)$$

This formulation naturally handles both material heterogeneity and evolving fracture as the free surface boundary conditions on $\partial\Omega_N$. For further discussions on the free surface boundary conditions and more general Neumann-type boundary conditions in peridynamics, we refer interested readers to [52, 54].

3 Optimization-Based Quadrature Rules

In this section, we elaborate the strong-form particle discretization of the nonlocal diffusion and peridynamics models introduced above. To obtain a unified formulation for both models, we rewrite (2) and (6) as a general heterogeneous nonlocal operator of the form:

$$\mathcal{L}_\delta[u](\mathbf{x}, t) := \int_{\mathcal{B}_\delta(\mathbf{x})} K(\mathbf{x}, \mathbf{y})(u(\mathbf{y}, t) - u(\mathbf{x}, t)) d\mathbf{y}, \quad \text{with } K(\mathbf{x}, \mathbf{y}) := \varpi(\mathbf{x}, \mathbf{y}) C(\mathbf{x}, \mathbf{y}) \gamma(\mathbf{x}, \mathbf{y}). \quad (12)$$

Here, γ is the nonlocal kernel satisfying (3), $\varpi(\mathbf{x}, \mathbf{y})$ is a general two-point function corresponding to the (heterogeneous) material properties, and $C(\mathbf{x}, \mathbf{y})$ corresponds to a two-point (tensor) function which is designed to guarantee the consistency to the desired local limit. In nonlocal diffusion problems, we have $\varpi(\mathbf{x}, \mathbf{y}) := A(\mathbf{x}, \mathbf{y})$ and $C(\mathbf{x}, \mathbf{y}) := 2$, which corresponds to the diffusion property. In bond-based peridynamics, $\varpi(\mathbf{x}, \mathbf{y}) := \kappa(\mathbf{x}, \mathbf{y})$ and $C(\mathbf{x}, \mathbf{y}) := c \frac{(\mathbf{y} - \mathbf{x}) \otimes (\mathbf{y} - \mathbf{x})}{|\mathbf{y} - \mathbf{x}|^2}$, characterizing the average material properties and bond strengths between material points \mathbf{x} and \mathbf{y} .

Denoting u_δ and u_0 as the nonlocal and local analytical solution respectively, and $u_{\delta,h}$ as the numerical solution, in OBMeshfree we focus on two types of convergence:

$$\lim_{h \rightarrow 0} \|u_{\delta,h} - u_\delta\|_{L^2(\Omega)} = 0, \quad \text{and} \quad \lim_{h, \delta \rightarrow 0} \|u_{\delta,h} - u_0\|_{L^2(\Omega)} = 0. \quad (13)$$

The first type of convergence indicates that the numerical discretization method is consistent with the nonlocal problem, while the second type shows that the nonlocal numerical solution preserves the correct local limit, or equivalently, the numerical scheme is

asymptotically compatible. To maintain an easily scalable implementation, in asymptotic compatibility studies we assume δ to be chosen such that the ratio $\frac{\delta}{h}$ is bound by a constant as $\delta \rightarrow 0$, restricting ourselves to the “ δ -convergence” scenario [72]. In the following sections, we will first introduce the spatial and temporal discretization methods for nonlocal diffusion and peridynamics problems with full Dirichlet-type boundary conditions. Then, we incorporate the bond breaking mechanism and the free surface formulation, to provide a fully discretized framework for bond-based peridynamics including the damage criteria and the handling of free surfaces created by evolving fracture.

3.1 Spatial Discretization

Assume that the whole interaction domain, Ω_D , is discretized into a collection of points

$$\chi_h = \{\mathbf{x}_i\}_{i=1}^M \subset \Omega \cup \mathcal{B}\Omega,$$

we seek for numerical solutions such that $u_i \approx u(\mathbf{x}_i)$. Recall the definitions [73] of fill distance $h_{\chi_h, \Omega} = \sup_{\mathbf{x}_i \in \Omega} \min_{\mathbf{x}_j \in \chi_h \setminus \{\mathbf{x}_i\}} \|\mathbf{x}_i - \mathbf{x}_j\|_2$ and separation distance $q_{\chi_h} = \frac{1}{2} \min_{i \neq j} \|\mathbf{x}_i - \mathbf{x}_j\|_2$, for simplicity we drop subscripts and simply write h and q . In this work, we assume that χ_h is *quasi-uniform*, namely that there exists a constant $C_q > 0$, such that $q \leq h \leq C_q q$.

Then, we seek to generate consistent meshfree quadrature rules of the form

$$\mathcal{L}_\delta[u](\mathbf{x}_i, t) \approx \mathcal{L}_{\delta, h}[u](\mathbf{x}_i, t) := \sum_{j \neq i} K(\mathbf{x}_i, \mathbf{x}_j)(u(\mathbf{x}_j, t) - u(\mathbf{x}_i, t))\omega_{ij}. \tag{14}$$

Here, $\{\omega_{ij}\}_{\mathbf{x}_j \in \mathcal{B}_\delta(\mathbf{x}_i)}$ is a collection of to-be-determined quadrature weights corresponding to a neighborhood of collocation point \mathbf{x}_i , which will be constructed through an optimization-based approach to ensure consistency guarantees. Specifically, we seek quadrature weights for integrals supported on balls of the form

$$I[q] := \int_{\mathcal{B}_\delta(\mathbf{x}_i)} q(\mathbf{x}_i, \mathbf{y})d\mathbf{y} \approx I_h[q] := \sum_{\mathbf{x}_j \in \chi_h \cap \mathcal{B}_\delta(\mathbf{x}_i) \setminus \{\mathbf{x}_i\}} q(\mathbf{x}_i, \mathbf{x}_j)\omega_{ij}, \tag{15}$$

where the subscript i in $\{\omega_{ij}\}$ denote that we seek a different family of quadrature weights for different subdomains $\mathcal{B}_\delta(\mathbf{x}_i)$. These weights are then generated from the following optimization problem

$$\min_{\{\omega_{ij}\}} \sum_{\mathbf{x}_j \in \chi_h \cap \mathcal{B}_\delta(\mathbf{x}_i) \setminus \{\mathbf{x}_i\}} \omega_{ij}^2 \gamma_\delta(\mathbf{x}_i, \mathbf{x}_j) \quad \text{such that,} \quad I_h[q] = I[q] \quad \forall q \in V_{h, \mathbf{x}_i}, \tag{16}$$

where $V_{h, \mathbf{x}_i} = \left\{ q(\mathbf{y} - \mathbf{x}_i) = p(\mathbf{y} - \mathbf{x}_i)\gamma_\delta(\mathbf{x}_i, \mathbf{y})C(\mathbf{x}_i, \mathbf{y}) \mid p \in \mathbb{P}_n(\mathbb{R}^d) \text{ such that } \int_{\mathcal{B}_\delta(\mathbf{x}_i)} q(\mathbf{y} - \mathbf{x}_i)d\mathbf{y} < \infty \right\}$, denotes the space of functions which should be integrated exactly. $\mathbb{P}_n(\mathbb{R}^d)$ is the space of n -th order polynomials, and $C(\mathbf{x}, \mathbf{y})$ is given as in (12).

For each material point $\mathbf{x}_i \in \Omega \cap \chi_h$, we denote the total number of to-be-determined quadrature weights ω_{ij} as M_i . To solve for the optimization problem (16), we formulate it as a saddle point problem

$$\begin{bmatrix} \mathbf{W} & \mathbf{B}^\top \\ \mathbf{B} & \mathbf{0} \end{bmatrix} \begin{bmatrix} \boldsymbol{\omega} \\ \boldsymbol{\lambda} \end{bmatrix} = \begin{bmatrix} \mathbf{0} \\ \mathbf{g} \end{bmatrix}, \tag{17}$$

where $\mathbf{W} \in \mathbb{R}^{M_i \times M_i}$ is a diagonal matrix with the diagonal element determined by $W_{jj} = 2\gamma_\delta(\mathbf{x}_i, \mathbf{x}_j)$, $\boldsymbol{\omega} \in \mathbb{R}^{M_i}$ are the vector of quadrature weights ω_{ij} , and $\boldsymbol{\lambda} \in \mathbb{R}^{\dim(V_{h,\mathbf{x}_i})}$ are a set of Lagrange multipliers. $\mathbf{B} \in \mathbb{R}^{M_i \times \dim(V_{h,\mathbf{x}_i})}$ consists of the reproducing function evaluated at the quadrature points, satisfying $B_{\alpha j} = q_\alpha(\mathbf{x}_j - \mathbf{x}_i)$, for $q_\alpha \in V_{h,\mathbf{x}_i}$ and $\mathbf{x}_j \in \chi_h \cap B_\delta(\mathbf{x}_i) \setminus \{\mathbf{x}_i\}$. $\mathbf{g} \in \mathbb{R}^{\dim(V_{h,\mathbf{x}_i})}$ consists of the integral of the reproducing functions over the ball, satisfying $\mathbf{g}_\alpha = I[q_\alpha]$. By eliminating the constraints, the quadrature weights can be obtained by solving

$$\boldsymbol{\omega} = \mathbf{W}^{-1} \mathbf{B}^\top (\mathbf{B} \mathbf{W}^{-1} \mathbf{B}^\top)^{-1} \mathbf{g}. \tag{18}$$

We note that the application of this quadrature does not require a background grid and is therefore truly meshfree. Moreover, the quadrature weights only need to be obtained once, using a list of neighbors lying within $B_\delta(\mathbf{x})$. In fact, in OBMeshfree weights are obtained as a preprocessing step, by solving a small local optimization problem requiring only the inversion of a small linear system in (18) for each \mathbf{x}_i .

Substituting the quadrature rule (14), the nonlocal diffusion operator $\mathcal{L}_{D\delta}$ and the bond-based peridynamics operator $\mathcal{L}_{P\delta}$ can be respectively discretized as:

$$(\mathcal{L}_{D\delta,h} u)_i := 2 \sum_{\mathbf{x}_j \in \chi_h \cap B_\delta(\mathbf{x}_i) \setminus \{\mathbf{x}_i\}} A(\mathbf{x}_i, \mathbf{x}_j) \gamma_\delta(|\mathbf{x}_i - \mathbf{x}_j|) (u_i - u_j) \omega_{ij}, \tag{19}$$

$$(\mathcal{L}_{P\delta,h} \mathbf{u})_i := c \sum_{\mathbf{x}_j \in \chi_h \cap B_\delta(\mathbf{x}_i) \setminus \{\mathbf{x}_i\}} \kappa(\mathbf{x}_i, \mathbf{x}_j) \gamma_\delta(|\mathbf{x}_i - \mathbf{x}_j|) \frac{(\mathbf{x}_j - \mathbf{x}_i) \otimes (\mathbf{x}_j - \mathbf{x}_i)}{|\mathbf{x}_j - \mathbf{x}_i|^2} (\mathbf{u}_i - \mathbf{u}_j) \omega_{ij}. \tag{20}$$

As verified in [45, 51–53], the above quadrature rule is able to obtain a compatible discretization that achieves both the consistency with the nonlocal analytical solution and the asymptotic compatibility to the local limit. In the following, we briefly list the theoretical analysis results provided in [45, 51]. For analysis, we denote

$$K(\mathbf{x}, \mathbf{y}) = \frac{N(\mathbf{x}, \mathbf{y})}{\delta^{d+2-s} |\mathbf{x} - \mathbf{y}|^s}, \tag{21}$$

where the numerator satisfies $N(\mathbf{x}, \mathbf{y}) \leq C_N$ for all $\mathbf{y} \in B_\delta(\mathbf{x})$.

For the asymptotic compatibility to the local limit, as shown in [45], the optimization-based quadrature rule has the following truncation error estimates:

Theorem 1 (Truncation Estimates with Fixed h/δ) *Consider a fixed ratio h/δ and assume that both $N(\mathbf{x}, \mathbf{y})$ and $u(\mathbf{x})$ are sufficiently smooth, i.e., $N(\mathbf{x}, \mathbf{y}) \in C^{n+2}(\overline{(\Omega_D)^2})$ and $u(\mathbf{x}) \in C^{n+2}(\overline{\Omega_D})$. For any $\mathbf{x}_i \in \chi_h \cap \Omega$, the quadrature weights obtained from (16) with $n > d + s - 3$ would satisfy the following pointwise error estimate, with a constant $C > 0$ independent of δ and \mathbf{x}_i :*

$$\left| \int_{B_\delta(\mathbf{x}_i)} K(\mathbf{x}_i, \mathbf{y}) u(\mathbf{y}) d\mathbf{y} - \sum_{\mathbf{x}_j \in \chi_h \cap B_\delta(\mathbf{x}_i) \setminus \{\mathbf{x}_i\}} K_{ij} u_j \omega_{ij} \right| < C \delta^{n-1}.$$

For the convergence to the nonlocal analytical solution, following [51], we further require that $s < d$. Moreover, χ_h is assumed to be a uniform Cartesian grid:

$$\chi_h := \{(k_{(1)}h, \dots, k_{(d)}h) \mid \mathbf{k} = (k_{(1)}, \dots, k_{(d)}) \in \mathbb{Z}^d\} \cap \Omega_D,$$

where h is the spatial grid size. Then, the optimization-based quadrature rule has the following truncation error estimates with fixed δ and vanishing h :

Theorem 2 (Truncation Estimates with Fixed δ) *Consider a fixed δ and assume that both $N(\mathbf{x}, \mathbf{y})$ and $u(\mathbf{x})$ are sufficiently smooth, satisfying $N(\mathbf{x}, \mathbf{y}) \in C^4(\overline{(\Omega_D)^2})$ and $u(\mathbf{x}) \in C^1(\overline{\Omega_D})$. Then there exists a constant $C_{pos} < 1$, such that for $h < C_{pos}\delta$, the quadrature weights obtained from (16) with $n = 3$ would satisfy the following pointwise error estimate, with the generic constant $C > 0$ independent of h but may dependent on δ :*

$$\left| \int_{B_\delta(\mathbf{x}_i)} K(\mathbf{x}_i, \mathbf{y})u(\mathbf{y})d\mathbf{y} - \sum_{\mathbf{x}_j \in \chi_h \cap B_\delta(\mathbf{x}_i) \setminus \{\mathbf{x}_i\}} K_{ij}u_j\omega_{ij} \right| < Ch^{\min(1, d-s)}.$$

With the above truncation error estimates, the following convergence properties can be proved for static nonlocal diffusion problems, with detailed proof can be found in [51]:

Theorem 3 (Asymptotic Compatibility to the Analytical Local Diffusion Problems) *Consider uniform Cartesian grids and $s < d$. Assume that $A(\mathbf{x}, \mathbf{y}) \in C^4(\overline{(\Omega_D)^2})$, $a(\mathbf{x}) \in C^\infty(\Omega)$, $\Omega_D \in C^1$, and the analytical local diffusion solution $u_0 \in C^4(\overline{\Omega_D})$. When applying the boundary condition $u_D(\mathbf{x}_i) = u_0(\mathbf{x}_i)$ for $\mathbf{x}_i \in \chi_h \cap \mathcal{B}\Omega_D$, there exists a $\delta_0 > 0$ and $C_{pos} < 1$, such that for any $0 < \delta < \delta_0$ and fixed ratio $h/\delta < C_{pos}$, the meshfree quadrature rule with $n = 3$ is asymptotically compatible for nonlocal diffusion problems, i.e.,*

$$\|u_{\delta, h} - u_0\|_{L^\infty(\chi_h)} \leq C\delta^2, \tag{22}$$

where C is a generic constant independent of δ and h .

Theorem 4 (Convergence to the Analytical Nonlocal Diffusion Solution) *Consider uniform Cartesian grids and $s < d$. Assume that $A(\mathbf{x}, \mathbf{y}) \in C^4(\overline{(\Omega_D)^2})$, the analytical nonlocal diffusion solution $u_\delta(\mathbf{x}) \in C^1(\overline{\Omega_D})$, $a(\mathbf{x}) \in C^\infty(\Omega)$ and $\Omega_D \in C^1$, then there exists a $\delta_0 > 0$ and $C_{pos} < 1$, such that for a fixed δ satisfying $0 < \delta < \delta_0$ and $h < C_{pos}\delta$, the following convergence property holds for the meshfree quadrature rule with $n = 3$:*

$$\|u_{\delta, h} - u_\delta\|_{L^\infty(\chi_h)} \leq Ch^{\min(1, d-s)}, \tag{23}$$

where C is a generic constant independent of h but may depends on δ .

3.2 Temporal Discretization

In this section we introduce the discretization methods in time, and demonstrate the fully discretized methods for nonlocal diffusion and peridynamics problems with Dirichlet-type boundary conditions. Although in the demonstrating examples of Sect. 5 we mostly focus on static nonlocal problems (except the validation problem of the Kalthoff-Winkler

experiment), the options and codes of dynamic problems are implemented in OBMeshfree, which can be readily used following the instruction provided in Sect. 4.

For the dynamic nonlocal diffusion model (4), the backward Euler method is employed. With time step size Δt and the approximated solution at the m -th time step, u_i^m , the solution at the $m + 1$ -th time step is solved via:

$$\begin{cases} \frac{\rho}{\Delta t} u_i^{m+1} - (\mathcal{L}_{D\delta,h} u)_i^{m+1} = f(x_i, (m + 1)\Delta t) + \frac{\rho}{\Delta t} u_i^m, & \text{for } x_i \text{ in } \Omega \cap \chi_h, \\ u_i^{m+1} = u_D(x_i, (m + 1)\Delta t), & \text{for } x_i \text{ in } \mathcal{B}\Omega_D \cap \chi_h, \\ u_i^0 = \phi(x_i), & \text{for } x_i \in \Omega_D \cap \chi_h, \end{cases} \quad (24)$$

where $\mathcal{L}_{D\delta,h}$ is the discrete nonlocal diffusion operator as defined in (19), $u_D(x_i)$ is the prescribed Dirichlet boundary condition, and ϕ is the initial value.

For the dynamic peridynamics model, to discretize in time we also apply the backward time stepping scheme. With time step size Δt , at the $(m + 1)$ -th time step we solve for the displacement $u_i^{m+1} \approx u(x_i, (m + 1)\Delta t)$ following:

$$\begin{cases} \frac{\rho}{\Delta t^2} u_i^{m+1} - (\mathcal{L}_{P\delta,h} u)_i^{m+1} = f(x_i, (m + 1)\Delta t) + \frac{\rho}{\Delta t^2} (2u_i^m - u_i^{m-1}), & \text{for } x_i \text{ in } \Omega \cap \chi_h, \\ u_i^{m+1} = u_D(x_i, (m + 1)\Delta t), & \text{for } x_i \text{ in } \mathcal{B}\Omega_D \cap \chi_h, \\ u_i^0 = \phi(x_i), \quad u_i^1 = \psi(x_i), & \text{for } x_i \in \Omega_D \cap \chi_h, \end{cases} \quad (25)$$

where $\mathcal{L}_{P\delta,h}$ is the discretized nonlocal operator as defined in (20), u_D is the given Dirichlet-type boundary condition, and ϕ, ψ are the initial displacement field at the first two time steps.

3.3 Peridynamics with Free Surfaces and Evolving Fracture

In this section we extend OBMeshfree, to handle peridynamics models with free surfaces and fracture. For a given point x_i and the horizon δ , a bond is associated with each neighbor point $x_j \in B_\delta(x_i)$, and the weight ω_{ij} is associated with this bond. In the meshfree formulation, the fracture is captured by evolving free surfaces implicitly via the breaking of bonds. When fracture occurs, it creates new surfaces when the free surface boundary conditions are applied. These new free surfaces will also be added into the set of Neumann-type boundary, $\partial\Omega_N$. That means, $\partial\Omega_N$ evolves with fracture. Instead of parameterizing the $\partial\Omega_N$ and evolve its formulation with time, in OBMeshfree the boundary $\partial\Omega_N$ is naturally represented by breaking bonds. In particular, when the change of displacement on material point x_j may have an impact on the displacement at x_i , we call their bond as ‘‘intact’’, and set the corresponding state function value $\theta(x_i, x_j, t)$ as 1. On the other hand, when the bond between x_i and x_j intersects the surface $\partial\Omega_N$, and/or the bond stretch $S(x_i, x_j, \tau)$ has exceeded the critical bond stretch threshold $S_0(x, y)$ at some time instant $\tau < t$, the bond is considered ‘‘broken’’ and we set $\theta(x_i, x_j, t)$ as 0. In particular, at the m -th time step we set:

$$\theta_{ij}^m = \begin{cases} 1, & \text{if } x_j \in B_\delta(x_i) \cap \Omega_D \text{ and } S(x_i, x_j, l\Delta t) \leq S_0(x_i, x_j), \quad \forall l = 1, \dots, m, \\ 0, & \text{otherwise,} \end{cases} \quad (26)$$

Applying the above formulation in (11), at the m -th dynamic step, we seek for solutions of the displacement $u_i^m \approx u(x_i, m\Delta t)$ through the following meshfree scheme:

$$\begin{aligned} & \frac{\rho}{\Delta t^2} \mathbf{u}_i^{m+1} - c \sum_{x_j \in \mathcal{X}_h \cap B_\delta(x_i) \setminus \{x_i\}} \kappa(x_i, x_j) \gamma_\delta(|x_i - x_j|) \frac{(x_j - x_i) \otimes (x_j - x_i)}{|x_j - x_i|^2} (\mathbf{u}_i^{m+1} - \mathbf{u}_j^{m+1}) \theta_{ij}^m \omega_{ij} \\ & = \mathbf{f}(x_i, (m + 1)\Delta t) + \frac{\rho}{\Delta t^2} (2\mathbf{u}_i^m - \mathbf{u}_i^{m-1}), \quad \text{for } x_i \text{ in } \Omega \cap \mathcal{X}_h, \end{aligned} \tag{27}$$

$$\mathbf{u}_i^{m+1} = \mathbf{u}_D(x_i, (m + 1)\Delta t), \quad \text{for } x_i \text{ in } \mathcal{B}\Omega_D \cap \mathcal{X}_h, \tag{28}$$

$$\mathbf{u}_i^0 = \boldsymbol{\phi}(x_i), \quad \mathbf{u}_i^1 = \boldsymbol{\psi}(x_i), \quad \text{for } x_i \in \Omega_D \cap \mathcal{X}_h. \tag{29}$$

Note that because the evolving fracture creates new free surfaces, so $\partial\Omega_N$ and θ alter with u^{m+1} . In our implementation, we have been using the damage index, θ_{ij}^m , from the last time step, and the above algorithm can therefore be seen as a semi-implicit time integration approach. However, we point out the users can also implement a fully implicit approach by employing subiterations at each time step following [54], to capture the implicit coupling between the material response and the evolving geometry due to fracture evolution. First one can assume that no new bonds have been broken at the current time step and solve for the displacement field. Second, based on the displacement field, the damage criteria is evaluated and θ_{ij}^{m+1} is updated following (26) for each bond. If any bond meets the criteria of breaking, the displacement field will be solved again with new free surfaces. In [54], we repeat this procedure until no new broken bonds are detected, and finally proceed to the next time step.

Finally, the solution \mathbf{u}_i^{m+1} and the bond state function θ_{ij}^{m+1} are obtained at time step $m + 1$, we postprocess fracture evolution and identify cracks, by calculating the damage field $d_i^{m+1} \approx d(x_i, (m + 1)\Delta t)$ as

$$d_i^{m+1} = \frac{\sum_{x_j \in \mathcal{X}_h \cap B_\delta(x_i) \setminus x_i} (1 - \theta_{ij}^{m+1})}{\sum_{x_j \in \mathcal{X}_h \cap B_\delta(x_i) \setminus x_i} 1}, \tag{30}$$

which measures the weakening of material via the percentage of broken bonds in the neighborhood of x_i .

4 Using OBMeshfree

In this section we firstly overview the usage of OBMeshfree. For quick start, we refer the readers to Sect. 4.1. In order to further customize the examples, we then introduce the overall structure of the code and explain each.cpp file in detail in Sect. 4.3. One can find the most up-to-date version of OBMeshfree at https://github.com/youhq34/meshfree_quadrature_nonlocal.

4.1 OBMeshfree Usage and Workflow

Four cases are implement in this exemplar code. After downloading and extract the codes, users can compile the code using the following command

- ./make Nldiff for the static nonlocal diffusion problem, on a default domain $\Omega = [0, 1]^2$;
- ./make Nldiffd for the dynamic nonlocal diffusion problem, on a default domain $\Omega = [0, 1]^2$;
- ./make PD for the static bond-based peridynamics problem, on a default domain $\Omega = [0, 1]^2$;
- ./make KW for the dynamic bond-based peridynamics problem with evolving fracture, reproducing the Kalthoff-Winkler fracture experiment.

Then, the codes run with:

- ./nldiff.ex <#particles> <dhratio> <poly_order> <case> for the static nonlocal diffusion problem. Inputs are:
 - <#particles>: The number of uniform discretization points on each dimension.
 - <dhratio>: The ratio between δ and h .
 - <poly_order>: The highest polynomial order, n , to be exactly reproduced by the quadrature weights.⁵
 - <case>: A switcher for different experiment settings of Sect. 5. Here, 0 corresponds to the first example and 1 corresponds to the second example.
- ./nldiffd.ex <#particles> <dhratio> <poly_order> <dt> <timestep> for the dynamic nonlocal diffusion problem. The first three inputs are the same as in the static nonlocal diffusion problem. The last two inputs are:
 - <dt>: The time step size.
 - <timestep>: The total number of time steps to be simulated.
- ./PMB2D.ex <#particles> <dhratio> <poly_order> <perturbation> for the static bond-based peridynamics problem. The first three inputs are the same as in the nonlocal diffusion problem. The last input parameter is:
 - <perturbation>: The level of perturbation from a uniform grid, so as to create quasi-uniform discretization points. In particular, the Cartesian grids with grid size h are perturbed with a uniformly distributed random vector field $(\Delta x, \Delta y)$, $\Delta x, \Delta y \sim \mathcal{U}[-rh, rh]$. Here r controls the degree of perturbation, which is given by <perturbation>.
- ./KW.ex <#particles> <dhratio> <poly_order> <dt> <timestep> for the dynamic bond-based peridynamics problem with evolving fracture, with the same inputs as in the dynamic nonlocal diffusion problem.

⁵ Here, we point out that the highest polynomial order should be chosen based on the singularity of the kernel. Generally, one should set $n > d + s - 3$ according to the truncation estimates.

4.2 Software Components

gcc 7.5.0 or a newer version is required. The codes are built based on BLAS and LAPACK. Users might need to change the settings of BLAS and LAPACK libraries in Makefile.

4.3 Structure of the Code

The current version of OBMeshfree contains three folders, corresponding to nonlocal diffusion problems, bond-based peridynamics problems, and the Kalthoff-Winkler fracture experiment simulation, respectively.

- Under the folder `nonlocal_diffusion`, there are two `.cpp` files. `nonlocaldiff_static.cpp` is the script for static nonlocal diffusion problems, and `nonlocaldiff.cpp` is for dynamic nonlocal diffusion problems.
- Under the folder `bond-based-pd`, `PMB_2Dweight.cpp` provides the script for the static bond-based peridynamics model.
- Under the folder `Kalthoff-Winkler-test`, `KW_2Dweight_dynamic.cpp` is the script for the Kalthoff-Winkler fracture experiment, serving as an exemplar script for dynamic fracture problem with peridynamics, as well as a validation of OBMeshfree to realistic engineering applications.

In each folder, `vvector.h` provides the definitions for basic vector operations.

4.4 Description of the Code

In addition to the grid size h , the ratio between horizon/grid size, δ/h , the reproducing polynomial order n , and the time step size Δt , users can further customize the test examples and material properties based on their demands. In this section we will illustrate the structure of the scripts and the usage of each function.

4.4.1 Description of `nonlocal_static.cpp`

`nonlocal_static.cpp` provides numerical simulations for static nonlocal diffusion problems, and serves as a numerical verification for the consistency of numerical solutions to a user-defined analytical local/nonlocal limit. The structures are as follows.

- User defined functions:
 - `phi` defines the functions q in $V_{h,x}$, the finite dimensional function space OBMeshfree seeks to exactly reproduced by the quadrature weights.
 - `Iphi` defines the analytical integral of each q , which will be employed as the right hand side of the constraints in (16).
 - `inverse` is the function that calculates the inverse matrix, developed based on LAPACK.

- `u_exact` defines the analytical solution at point $\mathbf{x} = (x, y)$ when it is available, for the purpose of verifying the convergence. This analytical solution will be also used as initial conditions and boundary conditions.
 - `Ffun` defines the loading field $f(\mathbf{x})$ at point $\mathbf{x} = (x, y)$, with inputs \mathbf{x} and δ .
 - `diff_coef` defines the nonlocal diffusion coefficient at point $\mathbf{x} = (x, y)$ as the harmonic mean of the local diffusion coefficient, when studying the AC convergence. Users can also define the nonlocal diffusion coefficient field directly for a more general nonlocal model, as described below.
 - `nonlocal_diff_coef` defines the nonlocal diffusion coefficient $A(\mathbf{x}, y)$, taking a pair of 2D points, $(\mathbf{x}, y) = (x_1, x_2, y_1, y_2)$, as the input.
- `Preprocess` performs the main steps of `OBMeshfree`, i.e., generating the quadrature weights. `Preprocess` takes coordinates of the grids, number of grids, δ/h and the neighborhood list for each grid as inputs, and produces a list of quadrature weights ω_{ij} corresponding to each neighborhood point for all particles in the domain.
 - `Main` contains the complete procedure solving a static nonlocal diffusion problem. The steps are:
 1. Read in the number of discretization points in each direction as N and the ratio δ/h as `dhratio` from inputs.
 2. Set initial configuration, including x and y coordinates of the grids, and the analytical solution at each grid.
 3. Set neighborhood list for every particle.
 4. Generate quadrature weights via `Preprocess`.
 5. Assemble the stiffness matrix and corresponding forcing term for the particles in the computational domain $\Omega \cap \mathcal{X}_h$.
 6. Apply Dirichlet boundary condition for the particles in $\mathcal{B}\Omega_D \cap \mathcal{X}_h$.
 7. Solve for the linear system using `LAPACK` build-in functions.
 8. Compute the truncation error and the solution error based on the user-defined analytical solution.

4.4.2 Description of `nonlocaldiff.cpp`

`nonlocaldiff.cpp` runs dynamical simulations for nonlocal diffusion problems. It also provides the option to compare the numerical solutions with a user-defined analytical local/nonlocal limit. The structures are as follows.

- User defined functions:
 - `phi`, `Iphi`, `diff_coef` and `inverse` are defined the same as in Sect. 4.4.1.
 - `u_exact` defines the analytical solution at point $\mathbf{x} = (x, y)$ and time instant t .
 - `F_fun` defines the forcing term for the nonlocal diffusion equation at point $\mathbf{x} = (x, y)$ and time instant t .
- `Preprocess` generates the quadrature weights and also assembles the stiffness matrix.
- `Backward_Euler` is the function updating the solution at each time step, with the following steps:

1. Update the forcing term and the Dirichlet-type boundary condition for the current time instant t .
 2. Based on the solution at the previous time instant, $t - \Delta t$, solve the linear system via LAPACK build-in functions and update the solution at the current time instant t .
- `main` contains the complete procedure solving a dynamic nonlocal diffusion problem. The steps are:
1. Read in the number of discretization points in each direction as N , the ratio δ/h as `dhratio`, the time step size Δt as `dt`, and the total number of time steps as `timestep` from inputs.
 2. Set up the x and y coordinates of the grids, the initial condition, and the analytical solution at each discretization point.
 3. Set up the neighborhood list for every particle.
 4. Generate quadrature weights and assemble the stiffness matrix via `Preprocess`.
 5. Perform the iteration in time from step 1 to step `timestep`. At each time step, run `Backward_Euler`.
 6. Evaluate the solution error at the last time step.

4.4.3 Description of `PMB_2Dweight.cpp`

`PMB_2Dweight.cpp` performs the numerical verification for static bond-based peridynamics problem and provides the option to compare the numerical solutions with a user-defined analytical local/nonlocal limit. The structures are as follows.

- User defined functions:

- `phi` and `Iphi` are defined the same as in Sect. 4.4.1.
- `u_exact` and `v_exact` define the x - and y -components of the analytical displacement field at point $\mathbf{x} = (x, y)$, respectively.
- `E` defines the heterogeneous material property field, as the function of Young's modulus E at point $\mathbf{x} = (x, y)$. Then, the nonlocal modulus coefficient is defined as the harmonic mean of the local modulus coefficient.
- `fx_exact` and `fy_exact` defines the body force density components of the x - and y -directions at point $\mathbf{x} = (x, y)$, respectively.

- `Preprocess` generates the quadrature weights.

- `Main` performs the complete procedure solving a nonlocal static bond-based peridynamics problem. The steps are:

1. Read in the number of discretization points in each direction as N and the ratio δ/h as `dhratio` from inputs.
2. Set up the x and y coordinates of the grids and the analytical solution, if available, at each discretization point.
3. Set up the neighborhood list for every particle.
4. Generate quadrature weights via `Preprocess`.
5. Assemble the stiffness matrix and corresponding forcing term for the particles in the computational domain $\Omega \cap \mathcal{X}_h$.

6. Apply Dirichlet boundary condition for the particles in $\mathcal{B}\Omega_D \cap \mathcal{X}_h$.
7. Solve for the linear system using LAPACK build-in functions.
8. Compute the truncation error and the solution error.

4.4.4 Description of `KW_2Dweight_dynamic.cpp`

`KW_2Dweight_dynamic.cpp` performs numerical simulation to reproduce the Kalthoff-Winkler fracture experiment. It provides an exemplar simulation for dynamic bond-based peridynamics problem, and serves as a validation for the applicability of the approach to realistic problems. The structures are as follows.

– User define functions

- `phi`, `Iphi` are defined the same as in Sect. 4.4.1.
- `BoundaryID` assign each particle an ID, classifies the particles in $\mathcal{X}_h \cap \mathcal{B}\Omega$ into different regions for further processing.
- `Bulk` defines the bulk modulus of the material.
- `den` defines the density of the material.
- `smax` defines the critical bond stretch of the material.
- `u_bc` and `v_bc` define the x - and y -components of the displacement field at point $\mathbf{x} = (x, y)$ for imposing the boundary conditions in the Kalthoff-Winkler fracture experiment. `u_bc` and `v_bc` take the coordinate $\mathbf{x} = (x, y)$ and the user-defined `BoundaryID` of the particle \mathbf{x} as inputs, to impose the Dirichlet-type boundary condition on the top and the bottom of the object in the Kalthoff-Winkler fracture experiment.
- `fx` and `fy` define the body force density components of the x - and y -directions at point $\mathbf{x} = (x, y)$, respectively.

– `Preprocess` generates the quadrature weights.

– `Backward_Euler` is the function updating the solution at each time step, with the following steps:

1. Assemble the stiffness matrix using the new quadrature weights and the corresponding forcing term for the particles in the computational domain $\Omega \cap \mathcal{X}_h$.
2. Update the boundary condition for $\mathcal{B}\Omega \cap \mathcal{X}_h$ at time instance t .
3. Based on the solutions at the previous two time instants, $t - \Delta t$ and $t - 2\Delta t$, solve the linear system via LAPACK build-in functions and update the solution at the current time instant t .

– `main` contains the complete procedure for simulating the Kalthoff-Winkler fracture experiment. The steps are:

1. Read in the number of particles in y -direction as `N`, then set the number of particles in x -direction as `2N`. Read in the ratio δ/h as `dhratio`, the time step size as `dt`, and the total number of time steps to be simulated as `timestep` from input.
2. Set up material properties, including the bulk modulus `Bulk`, critical bond stretch `smax`, and material density `den` for bond-based peridynamics problems.

3. Set up the x and y coordinates of the grids and the initial condition at each discretization point.
4. Set up the neighborhood list for every particle.
5. Initialize the pre-notched crack by breaking any bond that intersects with the crack.
6. Generate quadrature weights through `Preprocess`.
7. For $m = 1 : \text{timestep}$
 - 7a. Examine the breaking bonds, update the bond state function values and the quadrature weights.
 - 7b. Run `Backward_Euler` to update the displacement field.
 - 7c. Compute the damage field using the current solution
 - 7d. Save the damage and displacements field for post processing.

5 Numerical Examples

In this section, we will use manufactured solutions to test the consistency of OBMeshfree, by investigating the convergence of the numerical solution to the local and nonlocal limits. Four test problems are considered: a static nonlocal diffusion problem verifying the consistency to the analytical nonlocal limit, a static nonlocal diffusion problem verifying the AC convergence, a static bond-based peridynamics problem verifying the AC convergence, and a dynamic bond-based peridynamics problem reproducing the Kalthoff-Winkler fracture experiment.

We denote u_δ and u_0 as the nonlocal and local analytical solution respectively, and $u_{\delta,h}$ the numerical solution. In example 1, we investigate the convergence of numerical solutions to the nonlocal analytical solution with vanishing h and fixed δ by calculating

$$\|u_{\delta,h} - u_\delta\|_{L^2}, \text{ where the root-mean-square takes the form } \|F\|_{L^2} := \sqrt{\frac{\sum_{x_i \in \chi_h} |F(x_i)|^2}{\#(\chi_h)}},$$

serving as a numerical approximation of the error in the $L^2(\Omega)$ norm. Then in examples 2 and 3, we investigate the convergence of numerical solutions to the local analytical solution under the δ -convergence limit. The differences between the local limit and the nonlocal numerical solution are estimated via $\|u_{\delta,h} - u_0\|_{L^2}$. Last but not least, in example 4 we consider the Kalthoff-Winkler experiment, wherein the fracture dynamics driven by an impactor striking a pre-notched plate generates an experimentally reproducible crack pattern. These four cases demonstrate the ability of the discretization to resolve both static and dynamic problems.

In nonlocal diffusion examples, we set the kernel γ_δ as a constant without singularity, i.e., $s = 0$. In this case, we note due to the $O(\delta^2)$ discrepancy between local and nonlocal diffusion operators, $n = 3$ would provide the smallest polynomial space of V_{h,x_i} to achieve the optimal convergence rate $O(\delta^2)$ in AC tests. Moreover, we further point out that when the grid is uniform, one can equivalently set $n = 2$, since the constraint for odd-order polynomials are automatically guaranteed thanks to the symmetric properties. Hence, we set the default reproducing polynomial order for nonlocal diffusion examples as $n = 2$. As discussed in Theorems 1 and 2, an $O(\delta^2)$ discrepancy to the local limit under δ -convergence and an $O(h)$ error to the nonlocal limit are anticipated. In peridynamics examples, we employ a singular kernel γ_δ with singularity order $s = 1$, and investigate the performance of our solver when the grids are not fully uniform. In this case, we set $n = 3$ as the default

reproducing polynomial order, since the grids and quadrature weights in each $B_\delta(x)$ are no longer symmetric.

5.1 Examples on Nonlocal Diffusion Problems

In this section we numerically investigate the convergence properties of OBMeshfree, by studying its performance on two nonlocal diffusion examples with manufactured solutions. To verify the error bounds provided in Theorems 3 and 4, besides the l^2 error we further measure the discrepancy of numerical solution and analytical solution with the l^∞ error given by: $\|F\|_{l^\infty} := \max_{x_i \in \mathcal{X}_h} |F(x_i)|$, serving as a numerical approximation of the error in the $L^\infty(\Omega)$ norm.

5.1.1 Consistency to the Nonlocal Limit

Firstly, we test the consistency of numerical solutions to the nonlocal limit. Consider a static nonlocal diffusion problem on $\Omega = [0, 1]^2$ with nonlocal diffusion coefficient field

$$A(\mathbf{x}, \mathbf{y}) := A(x_1, x_2, y_1, y_2) = 5 + x_1 + y_1,$$

subjected to the Dirichlet-type boundary condition on $\mathcal{B}\Omega_D$:

$$u_D(\mathbf{x}) = u_D(x, y) := x^6 + y^6,$$

and a loading field on Ω :

$$f(x) = f(x, y) := (5 + 2x)\left(\frac{5}{32}\pi\delta^8 + \frac{15}{8}\pi\delta^6(x^2 + y^2) + \frac{15}{4}\pi\delta^4(x^4 + y^4)\right) + \left(\frac{5}{32}\pi\delta^8x + \frac{15}{6}\delta^6x^3 + \frac{3}{2}\pi\delta^4x^5\right).$$

This problem has a manufactured analytical nonlocal solution

$$u_\delta(\mathbf{x}) = u_\delta(x, y) = x^6 + y^6.$$

Firstly, we aim to verify Theorem 1, by calculating the solution error and truncation error of the discretized nonlocal operator with a fixed $\delta/h = 3.5$ and decreasing horizon size δ from $7/16$ to $7/256$. The results with reproducing polynomial orders $n = 2, 3, 4, 5$ are illustrated in Fig. 1, where we plot the solution error $\|u_{\delta,h} - u_\delta\|$ as well as the truncation

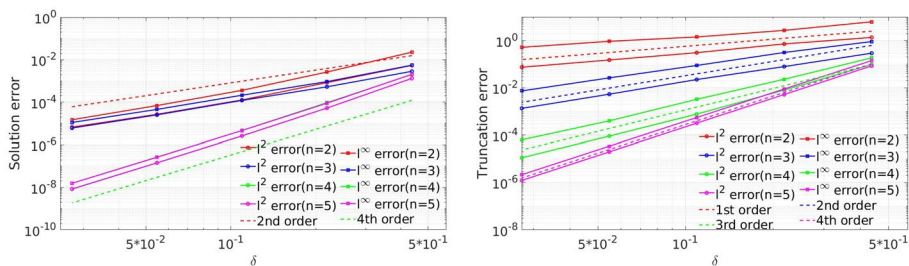


Fig. 1 Example 1: verifying the convergence of solution error $\|u_\delta - u_{\delta,h}\|$ (left) and truncation error $\|\mathcal{L}_{D\delta}[u_\delta] - \mathcal{L}_{D\delta,h}[u_\delta]\|$ (right) to the nonlocal limit, when taking $\delta \rightarrow 0$

error $\|\mathcal{L}_{D\delta}[u_\delta] - \mathcal{L}_{D\delta,h}[u_\delta]\|$ as functions of δ , for each value of n . We observe $O(\delta^{n-1})$ convergence in the truncation error, verified the estimate in Theorem 1. For the solution error, we observe $O(\delta^n)$ convergence for even n and $O(\delta^{n-1})$ convergence for odd n . This is probably caused by the symmetry of the odd-order polynomials on the ball when uniform grids are employed. Users can generate the above results using the script `nonlocaldiff_static.cpp`. As an instance, for grid size $h = 1/64$, horizon size $\delta = 3.5h$, and polynomial order $n = 5$, simulations run with the command `./nldiff.ex 64 3.5 5 0`, where the last argument corresponds to the case index for this example.

We now proceed to verify Theorems 2 and 4, by considering a fixed horizon size $\delta = 0.4375$ and decreasing the grid size h from $1/8$ to $1/128$. When taking the reproducing polynomial order $n = 2$ (which is equivalent to $n = 3$ due to the symmetry in uniform grids), the results are displayed in Fig. 2, illustrating an $O(h)$ convergence in both the truncation error and solution error. This result is consistent with the error estimates provided in Theorems 2 and 4. Users can generate these numerical results using the script `nonlocaldiff_static.cpp`. To keep the horizon size, δ , as a fixed value when decreasing h , the second and the third arguments should increase proportionally. For example, to fix the horizon size as $\delta = 0.4375$, for grid size $h = 1/8$ one should run the command `./nldiff.ex 8 3.5 3 0`, and for grid size $h = 1/16$ one should run `./nldiff.ex 16 7.0 3 0`.

5.1.2 Asymptotic Compatibility to the Local Limit

Herein, we study the AC consistency of the numerical solution, by considering a static nonlocal diffusion problem example with manufactured local limit. We study a heterogeneous nonlocal diffusion problem on $\Omega = [0, 1]^2$, with given local diffusion coefficient field

$$a(\mathbf{x}) = a(x, y) := 2 + \sin(x) \sin(y).$$

The object is subjected to Dirichlet-type boundary condition on $\mathcal{B}\Omega_D$ as:

$$u_D(\mathbf{x}) = u_D(x, y) := \cos(x) \cos(y)$$

and loading

$$f(\mathbf{x}) = f(x, y) := 4 \cos(x) \cos(y) + 4 \sin(x) \cos(x) \sin(y) \cos(y).$$

When taking the nonlocal diffusion coefficient field as the harmonic mean of $a(\mathbf{x})$ following (4), the nonlocal solution should converge to the analytical local solution

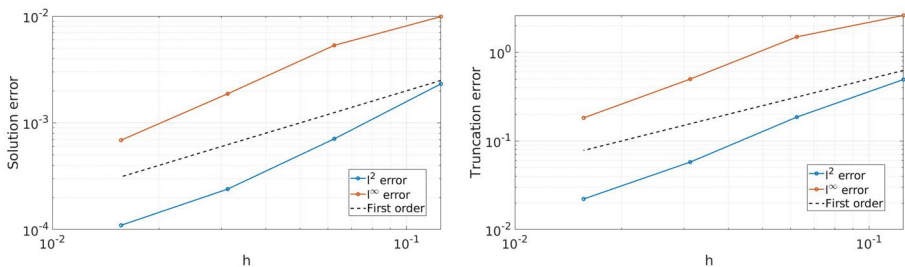


Fig. 2 Example 1: verifying the convergence of solution error $\|u_\delta - u_{\delta,h}\|$ (left) and truncation error $\|\mathcal{L}_{D\delta}[u_\delta] - \mathcal{L}_{D\delta,h}[u_\delta]\|$ (right) to the *nonlocal limit*, when taking a fixed δ and setting $h \rightarrow 0$

$$u_0(\mathbf{x}) = u_0(x, y) = \cos(x) \cos(y)$$

as $\delta \rightarrow 0$.

To present the numerical results of δ -convergence, we fix the ratio $\delta/h = 3.5$ and study the convergence of the numerical solution to the local limit with decreasing grid size h from $1/10$ to $1/160$. In this example we employ the reproducing polynomial order $n = 2$, which is equivalent to $n = 3$ due to the symmetry in uniform grids, and therefore is anticipated to provide the optimal convergence rate, $O(\delta^2)$, to the local limit. The solution error $\|u_{\delta,h} - u_0\|$ as well as the truncation error $\|\mathcal{L}_D[u_0] - \mathcal{L}_{D\delta,h}[u_0]\|$ are plotted as functions of δ in Fig. 3. In both l^2 and l^∞ norms, a $O(\delta^2)$ convergence is observed for the solution error and the truncation error, verifying the analysis in Theorem 3. To reproduce these results, users can run the script `nonlocaldiff_static.cpp`. Taking the case with grid size $h = 1/160$, reproducing polynomial order $n = 2$, and $\delta/h = 3.5$ as an instance, results are obtained with the command `./nldiff.ex 160 3.5 2 1`. Here, the last argument corresponds to the case index for this example.

5.2 Examples on Peridynamics

In this section we demonstrate two bond-based peridynamics examples using OBMeshfree. In the first example, we provide verification on a static example with manufactured local solution. To provide heuristic studies on the solution convergence rates, we measure discrepancy of numerical solution and analytical solution with the l^2 error. Then, in the second example we use the dynamic peridynamics code to reproduce the Kalthoff-Winkler fracture experiment, demonstrating the applicability of this approach to realistic engineering applications involving dynamic fracture. For the purpose of demonstration, we consider 2D problems under plane strain setting in all examples.

5.2.1 Asymptotic Compatibility to the Local Limit

In this section we consider the static bond-based peridynamics modeling for an object occupying the region $\Omega = [0, 1]^2$, whose material microstructure is characterized by a fixed Poisson ratio $\nu = 0.25$ and a local Young’s modulus field

$$E(\mathbf{x}) = E(x, y) := 2 + \sin(x) \sin(y).$$

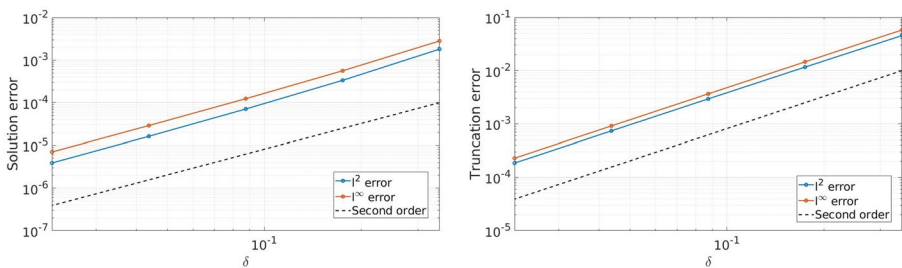


Fig. 3 Example 2: verifying the convergence of solution error $\|u_0 - u_{\delta,h}\|$ (left) and truncation error $\|\mathcal{L}_D[u_0] - \mathcal{L}_{D\delta,h}[u_0]\|$ (right) to the local limit, when taking $h, \delta \rightarrow 0$

Assume that the Dirichlet-type boundary condition

$$\mathbf{u}_D(\mathbf{x}) = \mathbf{u}_D(x, y) := [\sin(x) \sin(y), -\cos(x) \cos(y)]$$

is given for $\mathbf{x} \in \mathcal{B}\Omega_D$, and the object is subject to a body load

$$\mathbf{f}(\mathbf{x}) = \mathbf{f}(x, y) := \begin{bmatrix} -12C_1 \sin(x) \sin(y) + 4C_1 \cos(2x) \sin^2(y) + 4C_1 \cos(2y) \sin^2(x) \\ 12C_1 \cos(x) \cos(y) + 3C_1 \sin(2x) \sin(2y) \end{bmatrix}^T, \quad C_1 := 1/(2(1 + \nu)).$$

When taking the nonlocal modulus field as the harmonic mean of the local one, the bond-based peridynamics problem converges to the Navier equations [74–76] for linear elasticity:

$$-\mathcal{L}_P[\mathbf{u}](\mathbf{x}) = \mathbf{f}(\mathbf{x})$$

as $\delta \rightarrow 0$. Here,

$$\mathcal{L}_P[\mathbf{u}] := \frac{E}{2(1 + \nu)} \nabla \cdot (2\mathbf{E} + \text{tr}(\mathbf{E})\mathbf{I}), \tag{31}$$

where the strain tensor $\mathbf{E} := \frac{1}{2}(\nabla \mathbf{u} + (\nabla \mathbf{u})^T)$ and $\text{tr}(\mathbf{E})$ denotes its trace. Hence, with this example we aim to investigate if the numerical solution would converge to the following analytical local solution of (31):

$$\mathbf{u}_0(\mathbf{x}) = \mathbf{u}_0(x, y) := [\sin(x) \sin(y), -\cos(x) \cos(y)]$$

under the δ -convergence setting.

To study the AC convergence, in this example we fix $\delta/h = 3.5$ while decreasing the grid size h from $1/8$ to $1/128$, and calculate the discrepancy between our numerical solution and the analytical local limit. To demonstrate our meshfree approach in handling non-uniform grids, we first generate the uniform grid, then perturb the uniform grid points with $(\Delta x, \Delta y)$, where $\Delta x, \Delta y \sim \mathcal{U}[-rh, rh]$. Here, the perturbation ratio $r \in (0, 1)$ provides a metric for the effect of anisotropy in the underlying discretization. Two examples of perturbed grids are demonstrated in Fig. 4, corresponding to $r = 0.2$ and $r = 0.5$, respectively. For each perturbation ratio $r \in \{0.2, 0.5\}$, we generate 5 realizations of grids using different random seeds. To investigate the impact of

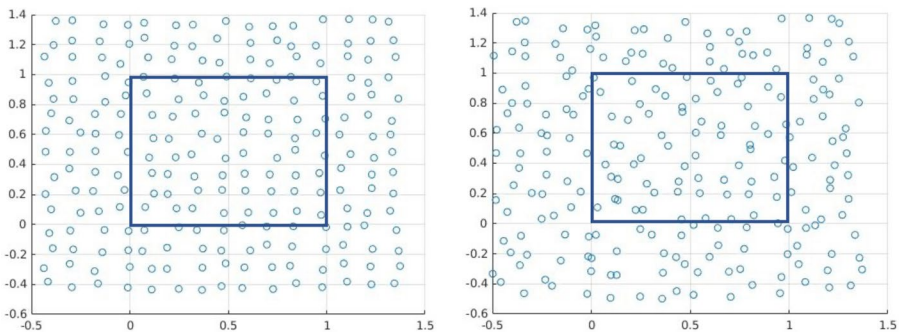


Fig. 4 Exemplar non-uniform grids generated for $\Omega \cup \mathcal{B}\Omega$, with the perturbation ratios $r = 20\%$ (left) and $r = 50\%$ (right). The computational domain $\Omega = [0, 1]^2$ is indicated by the blue box

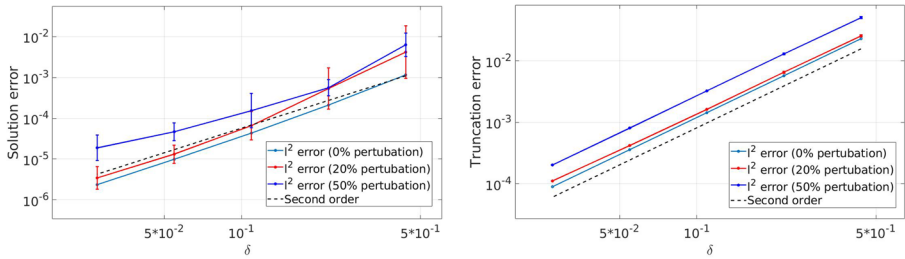


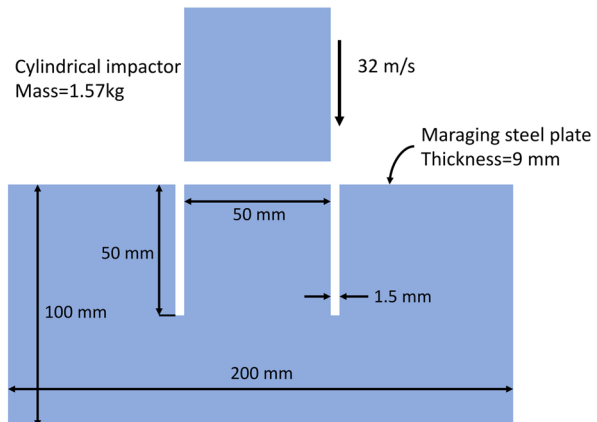
Fig. 5 Example 3: verifying the convergence of peridynamics solution error $\|u_0 - u_{\delta,h}\|$ (left) and truncation error $\|\mathcal{L}_p[u_0] - \mathcal{L}_{p\delta,h}[u_0]\|$ (right) to the *local limit*, when taking $h, \delta \rightarrow 0$ and perturbing the uniform grid with different levels of perturbation. Means and standard errors of 5 realizations are reported for each perturbation level

non-uniform grids, we record the solution and truncation errors for each realization, and report their means and standard errors versus the horizon size δ in Fig. 5. $O(\delta^2)$ convergence is observed in the truncation error for all perturbation levels. Here we notice that the standard errors of the right plot are almost invisible, showing that the truncation errors are not sensitive to perturbations in the discretization grids, possibly because they are dominated by the discrepancy from \mathbf{u} to the reproducing polynomial space instead of the interpolation error. For the solution error, we also observe $O(\delta^2)$ convergence to the local limit when using uniform grids, while the convergence rate slightly deteriorates as we increase the level of perturbation, possibly due to the effects of grid anisotropy on the stiffness matrix. To reproduce these results, users can run the script `PMB_2Dweight.cpp`. For grid size $h = 1/128$, $\delta/h = 3.5$, and perturbation level $r = 20\%$, as an instance, results are generated using the command `./PMB2D.ex 128 3.5 3 0.2'`.

5.2.2 Dynamic Fracture: Reproducing the Kalthoff-Winkler Experiment

We now consider a dynamic fracture problem where a steel plate is struck by a cylindrical impactor [77], which is the so-called Kalthoff-Winkler experiment. The plate is

Fig. 6 Experimental setup for the Kalthoff-Winkler experiment. The figure is adapted from [36]



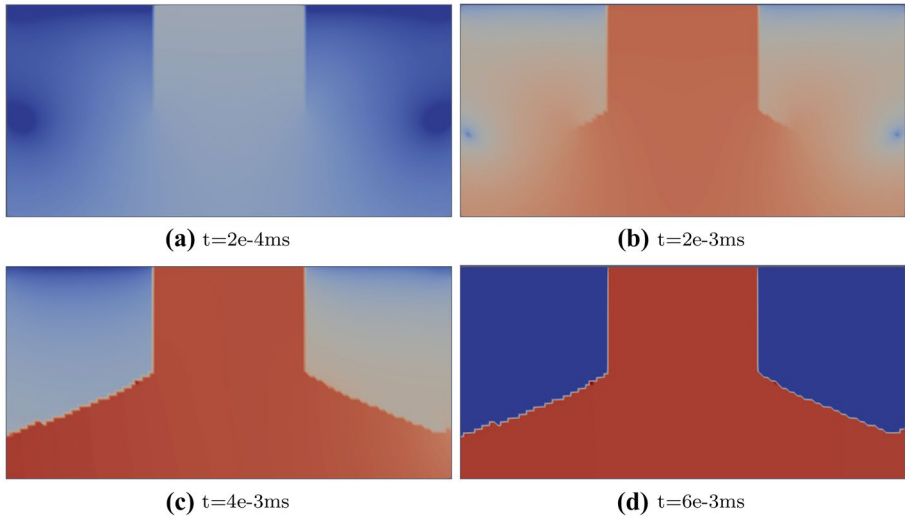


Fig. 7 The evolution of the displacement field for the Kalthoff-Winkler fracture experiment, after 1, 50, 100 and 150 time steps. The logarithmic value of displacement magnitude ($\log_{10} |u|$) is colored for plot

pre-notched, and crack will grow from the pre-notch tips upon an impact. Experiments show that the fracture pattern behaves differently depending on the regimes governed by the impactor velocity. In this example, we employ parameters given in Fig. 6, which is also consistent with those investigated previously in a particle-based peridynamics model [36]. Under such a setting, experimentally it was observed that a reproducible 68° angel is formed by the growing crack and the initial vertical pre-notch [77]. With this example, we aim to validate if our OBMeshfree is capable to capture the evolving fracture and reproducing the crack pattern.

In this example, to model the impact, $u = [0, -32t]$ is imposed between the two notches, as depicted in Fig. 6. Then, on the rest regime of the top of the plate, a homogeneous Dirichlet boundary conditions $u = [0, 0]$ is applied. All other boundaries are treated as free surfaces, hence any bonds across those surfaces are set as broken following Sect. 5.2.2. For the material

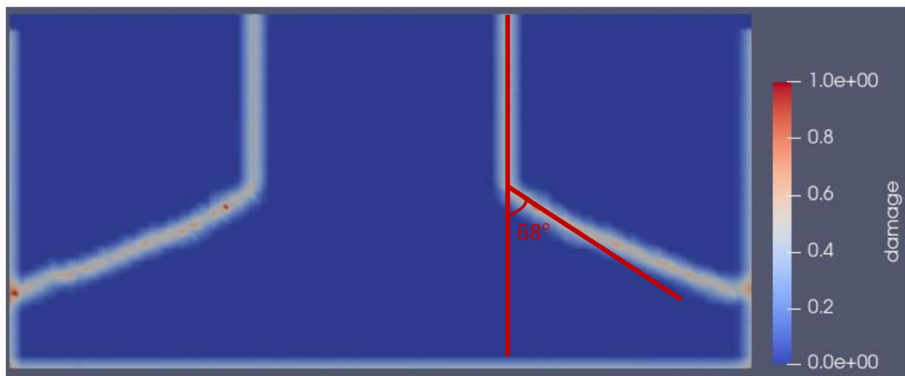


Fig. 8 Crack pattern for Kalthoff-Winkler experiment when taking $h = 0.15625$ cm and $\delta = 3.0h$ at time $t = 6e-3$ ms, successfully reproduced the 68° crack angle as reported in [36, 77]

properties, we employ the settings employed in [36]. In particular, the plate has a density $8e-3 \text{ kg/m}^3$, an elastic modulus of 191 GPa, a yield strength of 2000 MPa, and a fracture toughness of $90 \text{ MPa m}^{1/2}$. The above material properties yield a bond breaking criteria of $S_0 = 0.0099/\sqrt{\delta}$ following (9). In our code, the spatial unit is unified as cm, the temporal unit is unified as ms, and weight unit is unified as kg.

In Fig. 7 we illustrate the evolution of simulated displacement field at four time instances: $t=2e-4 \text{ ms}$, $t=2e-3 \text{ ms}$, $t=4e-3 \text{ ms}$, and $t=6e-3 \text{ ms}$. In this simulation a uniform grid with 64×128 particles, $\delta = 3.0h$ and time discretization size $\Delta t = 2e-4 \text{ ms}$ are employed. At the end of the simulation, three fragments remain due to the crack. In Fig. 8 we further illustrate the fracture pattern, whose fragment shape reproduces the experimentally observed 68° crack angle at the pre-notch tip. The results in this section are generated based on the script `KW_2Dweight_dynamic.cpp`. Users can reproduce these results by running the command `./KW.ex 64 3.0 3 2e-4 500`.

Remark 1 To fully resolve the transient dynamics of the problem in [78], we may define the CFL condition number $C_{CFL} := \frac{C_R \Delta t}{h}$, where C_R is the Rayleigh speed calculated following [79]. When $C_{CFL} \leq \frac{1}{2}$, we fully resolve the transient dynamics of the problem. In this example, our settings are corresponding to $C_{CFL} \approx 0.4$. For further results with different CFL condition numbers, we refer interested readers to [45], where both fully resolved dynamics ($C_{CFL} \leq \frac{1}{2}$) and implicit solution of wave propagation ($C_{CFL} > 1$) were investigated.

6 Conclusion

In this work, we have developed an open-source software called OBMeshfree for mesh-free analysis on nonlocal problems. The program is developed based on an optimization-based quadrature rule and consists of a set of routines for generating quadrature weights on a neighborhood of each material point, discretizing two-dimensional nonlocal diffusion and peridynamics operators, performing integrating in time, handling material heterogeneity and evolving fracture, and calculating solution and truncation errors in cases with manufactured solutions. Benchmark problems are presented to verify the convergence, efficiency, and robustness properties of the meshfree discretization method implemented in OBMeshfree, under both uniform and highly non-uniform nodal distributions. Our method features a unified mathematical workflow for handling material heterogeneity and evolving material fracture, and it is able to provably obtain high-order convergence to both local and nonlocal limits. With sufficient regularity assumptions on the solution and material property fields, the approach is able to obtain $O(h)$ and $O(\delta^2)$ convergences to the nonlocal and local theory, respectively.

The open-source code can serve as an entry point for researchers who are interested in the computer implementation of the optimization-based quadrature rule employed in [45, 50–53], and the code can also be adopted as a rapid prototyping and testing tool for the simulations with nonlocal models. Although the linear diffusion and bond-based peridynamics problems are chosen as the model problem, the flexibility of the code allows the extension to solve more advanced nonlocal problems for various scientific and engineering applications. For example, since phase transformations and fracture are both nonlinear phenomena, a development of meshfree solver for nonlocal and nonlinear problems is also desired. We also point out that as a simple demonstration of our meshfree method, in the

current implementation stiffness matrices are assembled in dense format and solved using LAPACK. For the purpose of further improving the efficiency in large scale problems, one might consider employing sparse matrices and high-performance linear algebra routines such as ScaLAPACK [80].

Author Contribution YF: software, methodology, writing, validation, analysis, investigation, visualization. HY: software, methodology, investigation, data curation. YY: analysis, conceptualization, resources, funding acquisition, writing, supervision.

Funding The authors are supported by the National Science Foundation under award DMS 1753031, and the AFOSR grant FA9550-22-1-0197. Portions of this research were conducted on Lehigh University's Research Computing infrastructure partially supported by NSF Award 2019035.

Data Availability The source code is available at https://github.com/youhq34/meshfree_quadrature_nonlocal. Any further data that support the findings of this study are available from the corresponding author, Yue Yu, upon reasonable request.

Declarations

Ethical Approval The study involves no human nor animal participants.

Competing Interests The authors declare no competing interests.

References

1. Fan Y, You H, Yu Y (2022) Obmeshfree: an optimization-based quadrature rule for meshfree discretization of nonlocal diffusion and peridynamics models. https://github.com/youhq34/meshfree_quadrature_nonlocal
2. Bobaru F, Foster JT, Geubelle PH, Silling SA (2016) Handbook of peridynamic modeling. CRC Press
3. Du Q, Zhou K (2011) Mathematical analysis for the peridynamic nonlocal continuum theory. *ESAIM: Math Model Numerical Anal* 45(2):217–234
4. Emmrich E, Weckner O (2007) Analysis and numerical approximation of an integro-differential equation modeling non-local effects in linear elasticity. *Math Mech Solids* 12(4):363–384
5. Parks ML, Lehoucq RB, Plimpton SJ, Silling SA (2008) Implementing peridynamics within a molecular dynamics code. *Comput Phys Commun* 179(11):777–783
6. Seleson P, Parks ML, Gunzburger M, Lehoucq RB (2009) Peridynamics as an upscaling of molecular dynamics. *Multiscale Modeling & Simulation* 8(1):204–227
7. Silling SA (2000) Reformulation of elasticity theory for discontinuities and long-range forces. *J Mech Phys Solids* 48(1):175–209
8. Zimmermann M (2005) A continuum theory with long-range forces for solids. Ph.D. Thesis, Massachusetts Institute of Technology
9. Bažant ZP, Jirásek M (2002) Nonlocal integral formulations of plasticity and damage: Survey of progress. *J Eng Mech* 128(11):1119–1149
10. Du Q, Gunzburger M, Lehoucq RB, Zhou K (2013) A nonlocal vector calculus, nonlocal volume-constrained problems, and nonlocal balance laws. *Math Models Methods Appl Sci* 23(03):493–540
11. Benson DA, Wheatcraft SW, Meerschaert MM (2000) Application of a fractional advection-dispersion equation. *Water Resour Res* 36(6):1403–1412
12. Katiyar A, Agrawal S, Ouchi H, Seleson P, Foster JT, Sharma MM (2020) A general peridynamics model for multiphase transport of non-newtonian compressible fluids in porous media. *J Comput Phys* 402
13. Katiyar A, Foster JT, Ouchi H, Sharma MM (2014) A peridynamic formulation of pressure driven convective fluid transport in porous media. *J Comput Phys* 261:209–229
14. Schumer R, Benson DA, Meerschaert MM, Baeumer B (2003) Multiscaling fractional advection-dispersion equations and their solutions. *Water Resour Res* 39(1)
15. Schumer R, Benson DA, Meerschaert MM, Wheatcraft SW (2001) Eulerian derivation of the fractional advection-dispersion equation. *J Contam Hydrol* 48(1–2):69–88
16. Bates PW, Chmaj A (1999) An integrodifferential model for phase transitions: Stationary solutions in higher space dimensions. *J Stat Phys* 95(5):1119–1139

17. Chen C, Fife PC (2000) Nonlocal models of phase transitions in solids. *Adv Math Sci Appl* 10(2):821–849
18. Dayal K, Bhattacharya K (2006) Kinetics of phase transformations in the peridynamic formulation of continuum mechanics. *J Mech Phys Solids* 54(9):1811–1842
19. Buades A, Coll B, Morel JM (2010) Image denoising methods. A new nonlocal principle. *SIAM Rev* 52(1):113–147
20. D’Elia M, De Los Reyes JC, Miniguano-Trujillo A (2021) Bilevel parameter learning for nonlocal image denoising models. *J Math Imaging Vis* 63(6):753–775
21. Gilboa G, Osher S (2007) Nonlocal linear image regularization and supervised segmentation. *Multi-scale Model Simul* 6(2):595–630
22. Lou Y, Zhang X, Osher S, Bertozzi A (2010) Image recovery via nonlocal operators. *J Sci Comput* 42(2):185–197
23. Alali B, Lipton R (2012) Multiscale dynamics of heterogeneous media in the peridynamic formulation. *J Elast* 106(1):71–103
24. Askari E, Bobaru F, Lehoucq R, Parks M, Silling S, Weckner O (2008) Peridynamics for multiscale materials modeling. *J Phys: Conf Ser* 125:012078. IOP Publishing
25. Du Q, Engquist B, Tian X (2020) Multiscale modeling, homogenization and nonlocal effects: Mathematical and computational issues. *Contemp Math* 754:115–140
26. Seleson PD (2010) Peridynamic multiscale models for the mechanics of materials: Constitutive relations, upscaling from atomistic systems, and interface problems. Ph.D. Thesis, The Florida State University
27. Silling SA (2021) Propagation of a stress pulse in a heterogeneous elastic bar. *J Peridyn Nonlocal Model* 3(3):255–275
28. Silling SA, D’Elia M, Yu Y, You H, Fermen-Coker M (2022) Peridynamic model for single-layer graphene obtained from coarse-grained bond forces. *J Peridyn Nonlocal Model* 1–22
29. You H, Yu Y, Silling S, D’Elia M (2022) A data-driven peridynamic continuum model for upscaling molecular dynamics. *Comput Methods Appl Mech Eng* 389
30. Bakunin OG (2008) Turbulence and diffusion: Scaling versus equations. Springer Science & Business Media
31. Schekochihin AA, Cowley SC, Yousef TA (2008) MHD turbulence: Nonlocal, anisotropic, nonuniversal? In: IUTAM Symposium on Computational Physics and New Perspectives in Turbulence, pp 347–354. Springer
32. D’Elia M, Du Q, Gunzburger M, Lehoucq R (2017) Nonlocal convection-diffusion problems on bounded domains and finite-range jump processes. *Comput Methods Appl Math* 17(4):707–722
33. Meerschaert MM, Sikorskii A (2019) Stochastic models for fractional calculus. In: *Stochastic Models for Fractional Calculus*. de Gruyter
34. Metzler R, Klafter J (2000) The random walk’s guide to anomalous diffusion: a fractional dynamics approach. *Phys Rep* 339(1):1–77
35. Ha YD, Bobaru F (2011) Characteristics of dynamic brittle fracture captured with peridynamics. *Eng Fract Mech* 78(6):1156–1168
36. Silling SA (2001) Peridynamic modeling of the Kalthoff-Winkler experiment. Submission for the 2001 Sandia Prize in Computational Science
37. Tian X, Du Q (2014) Asymptotically compatible schemes and applications to robust discretization of nonlocal models. *SIAM J Numer Anal* 52(4):1641–1665
38. D’Elia M, Du Q, Glusa C, Gunzburger M, Tian X, Zhou Z (2020) Numerical methods for nonlocal and fractional models. Preprint at <http://arxiv.org/abs/2002.01401>
39. Du Q (2016) Local limits and asymptotically compatible discretizations. *Handbook of Peridynamic Modeling*, pp 87–108
40. Hillman M, Pasetto M, Zhou G (2020) Generalized reproducing kernel peridynamics: Unification of local and non-local meshfree methods, non-local derivative operations, and an arbitrary-order state-based peridynamic formulation. *Comput Part Mech* 7(2):435–469
41. Leng Y, Tian X, Trask N, Foster JT (2019) Asymptotically compatible reproducing kernel collocation and meshfree integration for nonlocal diffusion. Preprint at <http://arxiv.org/abs/1907.12031>
42. Pasetto M, Leng Y, Chen JS, Foster JT, Seleson P (2018) A reproducing kernel enhanced approach for peridynamic solutions. *Comput Methods Appl Mech Eng* 340:1044–1078
43. Seleson P, Littlewood DJ (2016) Convergence studies in meshfree peridynamic simulations. *Computers & Mathematics with Applications* 71(11):2432–2448
44. Tao Y, Tian X, Du Q (2017) Nonlocal diffusion and peridynamic models with neumann type constraints and their numerical approximations. *Appl Math Comput* 305:282–298
45. Trask N, You H, Yu Y, Parks ML (2019) An asymptotically compatible meshfree quadrature rule for nonlocal problems with applications to peridynamics. *Comput Methods Appl Mech Eng* 343:151–165

46. You H, Lu X, Trask N, Yu Y (2020) An asymptotically compatible approach for Neumann-type boundary condition on nonlocal problems. *ESAIM: Math Model Num Anal* 54(4):1373–1413
47. You H, Yu Y, Kamensky D (2020) An asymptotically compatible formulation for local-to-nonlocal coupling problems without overlapping regions. *Comput Methods Appl Mech Eng* 366
48. Bessa M, Foster J, Belytschko T, Liu WK (2014) A meshfree unification: Reproducing kernel peridynamics. *Comput Mech* 53(6):1251–1264
49. Silling SA, Askari E (2005) A meshfree method based on the peridynamic model of solid mechanics. *Comput Struct* 83(17–18):1526–1535
50. D’Elia M, Yu Y (2022) On the prescription of boundary conditions for nonlocal poisson’s and peridynamics models. In: *Research in Mathematics of Materials Science*, pp 185–207. Springer
51. Fan Y, Tian X, Yang X, Li X, Webster C, Yu Y (2021) An asymptotically compatible probabilistic collocation method for randomly heterogeneous nonlocal problems. *Journal of Computational Physics* 465: 111376
52. Fan Y, You H, Tian X, Yang X, Li X, Prakash N, Yu Y (2022) A meshfree peridynamic model for brittle fracture in randomly heterogeneous materials. *Comput Methods Appl Mech Eng* 399, <https://doi.org/10.1016/j.cma.2022.115340>
53. Foss M, Radu P, Yu Y (2022) Convergence analysis and numerical studies for linearly elastic peridynamics with dirichlet-type boundary conditions. *J Peridyn Nonlocal Model* 1–36
54. Yu Y, You H, Trask N (2021) An asymptotically compatible treatment of traction loading in linearly elastic peridynamic fracture. *Comput Methods Appl Mech Eng* 377
55. Lipton R (2014) Dynamic brittle fracture as a small horizon limit of peridynamics. *J Elast* 117(1):21–50
56. Bobaru F, Duangpanya M (2010) The peridynamic formulation for transient heat conduction. *Int J Heat Mass Transf* 53(19–20):4047–4059
57. Bucur C, Valdinoci E (2016) *Nonlocal diffusion and applications*, vol. 20. Springer
58. Du Q, Gunzburger M, Lehoucq RB, Zhou K (2012) Analysis and approximation of nonlocal diffusion problems with volume constraints. *SIAM Rev* 54(4):667–696
59. Metzler R, Klafter J (2004) The restaurant at the end of the random walk: Recent developments in the description of anomalous transport by fractional dynamics. *J Phys A: Math Gen* 37(31):R161
60. Neuman SP, Tartakovsky DM (2009) Perspective on theories of non-fickian transport in heterogeneous media. *Adv Water Resour* 32(5):670–680
61. Diehl P, Lipton R, Wick T, Tyagi M (2022) A comparative review of peridynamics and phase-field models for engineering fracture mechanics. *Comput Mech* 1–35
62. Diehl P, Prudhomme S, Lévesque M (2019) A review of benchmark experiments for the validation of peridynamics models. *J Peridyn Nonlocal Model* 1(1):14–35
63. Silling S, Lehoucq R (2010) Peridynamic theory of solid mechanics. *Adv Appl Mech* 44(1):73–166
64. Silling SA (2003) Dynamic fracture modeling with a meshfree peridynamic code. *Computational Fluid and Solid Mechanics* 2003:641–644
65. Bobaru F, Zhang G (2015) Why do cracks branch? A peridynamic investigation of dynamic brittle fracture. *Int J Fract* 196(1):59–98
66. Ha YD, Bobaru F (2010) Studies of dynamic crack propagation and crack branching with peridynamics. *Int J Fract* 162(1):229–244
67. Prakash N, Deng B, Stewart RJ, Smith CM, Harris JT (2022) Investigation of microscale fracture mechanisms in glass-ceramics using peridynamics simulations. *J Am Ceram Soc* 105(6):4304–4320
68. Yu Y, Bargas FF, You H, Parks ML, Bittencourt ML, Karniadakis GE (2018) A partitioned coupling framework for peridynamics and classical theory: Analysis and simulations. *Comput Methods Appl Mech Eng* 340:905–931
69. Mehrmashhadi J, Tang Y, Zhao X, Xu Z, Pan JJ, Van Le Q, Bobaru F (2018) The effect of solder joint microstructure on the drop test failure-a peridynamic analysis. *IEEE Trans Compon Packag Manuf Technol* 9(1):58–71
70. Nguyen HA, Wang H, Tanaka S, Oterkus S, Oterkus E (2021) An in-depth investigation of bimaterial interface modeling using ordinary state-based peridynamics. *J Peridyn Nonlocal Model* 1–27
71. Zhang H, Qiao P (2018) A state-based peridynamic model for quantitative fracture analysis. *Int J Fract* 211(1–2):217–235
72. Bobaru F, Yang M, Alves LF, Silling SA, Askari E, Xu J (2009) Convergence, adaptive refinement, and scaling in 1D peridynamics. *Int J Numer Meth Eng* 77(6):852–877
73. Wendland H (2004) *Scattered data approximation*, vol. 17. Cambridge University Press
74. Mengesha T (2012) Nonlocal Korn-type characterization of Sobolev vector fields. *Commun Contemp Math* 14(04):1250028

75. Mengesha T, Du Q (2014) The bond-based peridynamic system with dirichlet-type volume constraint. *Proc Roy Soc Edinburgh Sect A* 144(1):161–186
76. Mengesha T, Du Q (2014) Nonlocal constrained value problems for a linear peridynamic Navier equation. *J Elast* 116(1):27–51
77. Kalthoff J, Winkler S (1988) Failure mode transition at high rates of shear loading. *DGM Informationsgesellschaft mbH Impact Load Dyn Behav Mater* 1:185–195
78. Ren H, Zhuang X, Cai Y, Rabczuk T (2016) Dual-horizon peridynamics. *Int J Numer Meth Eng* 108(12):1451–1476
79. Graff KF (2012) *Wave motion in elastic solids*. Courier Corporation
80. Blackford LS, Choi J, Cleary A, D’Azevedo E, Demmel J, Dhillon I, Dongarra J, Hammarling S, Henry G, Petitet A et al (1997) *ScaLAPACK users’ guide*. SIAM
81. D’Elia M, Tian X, Yu Y (2020) A physically consistent, flexible, and efficient strategy to convert local boundary conditions into nonlocal volume constraints. *SIAM J Sci Comput* 42(4):A1935–A1949

Publisher’s Note Springer Nature remains neutral with regard to jurisdictional claims in published maps and institutional affiliations.

Springer Nature or its licensor (e.g. a society or other partner) holds exclusive rights to this article under a publishing agreement with the author(s) or other rightsholder(s); author self-archiving of the accepted manuscript version of this article is solely governed by the terms of such publishing agreement and applicable law.